Diffusion Model with Cross Attention as an Inductive Bias for Disentanglement

Tao Yang[1]*, **Cuiling Lan**[2]†, **Yan Lu**[2] , **Nanning Zheng**[1]†
yt14212@stu.xjtu.edu.cn,
[1]National Key Laboratory of Human-Machine Hybrid Augmented Intelligence,
National Engineering Research Center for Visual Information and Applications,
and Institute of Artificial Intelligence and Robotics,
Xi'an Jiaotong University,
[2]Microsoft Research Asia

Abstract

Disentangled representation learning strives to extract the intrinsic factors within observed data. Factorizing these representations in an unsupervised manner is notably challenging and usually requires tailored loss functions or specific structural designs. In this paper, we introduce a new perspective and framework, demonstrating that diffusion models with cross-attention itself can serve as a powerful inductive bias to facilitate the learning of disentangled representations. We propose to encode an image into a set of concept tokens and treat them as the condition of the latent diffusion model for image reconstruction, where cross-attention over the concept tokens is used to bridge the encoder and U-Net of diffusion model. We analyze that the diffusion process inherently possesses the time-varying information bottlenecks. Such an information bottlenecks and cross-attention act as strong inductive biases for promoting disentanglement. Without any regularization term in loss function, this framework achieves superior disentanglement performance on the benchmark datasets, surpassing all previous methods with intricate designs. We have conducted comprehensive ablation studies and visualization analyses, shedding a light on the functioning of this model. We anticipate that our findings will inspire more investigation on exploring diffusion model for disentangled representation learning towards more sophisticated data analysis and understanding.

1 Introduction

Disentangled representation learning strive to uncover and understand the underlying causal factors of observed data [Bengio et al., 2013, Higgins et al., 2018]. This is believed to possess immense potential to enhance a multitude of machine learning tasks, facilitating machines to attain better interpretability, superior generalizability, controlled generation, and robustness [Wang et al., 2022]. Over the years, the field of disentangled representation learning has attracted significant academic interest and many research contributions. Numerous methods, encompassing Variational Autoencoders (VAE) based techniques (such as β-VAE [Higgins et al., 2017, Burgess et al., 2018], FactorVAE [Kim and Mnih, 2018]), Generative Adversarial Networks (GAN) based approaches (such as InfoGAN [Chen et al., 2016], InfoGAN-CR [Lin et al., 2020]), along with others [Yang et al., 2021, Ren et al., 2021], have have been proposed to advance this field further.

---

*Work done during internships at Microsoft Research Asia.

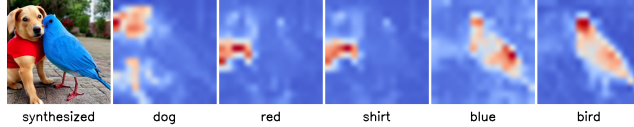†Corresponding authors: culan@microsoft.com; nnzheng@mail.xjtu.edu.cn.

Figure 1: Average attention map across all time steps in stable diffusion. We draw inspiration from the process of text-to-image generation using a diffusion model with cross-attention. Utilizing the highly 'disentangled' words as the condition for image generation, the cross-attention maps observed from the diffusion model exhibit a strong text semantic and spatial alignment, indicating the model is capable of incorporating each individual word into the generation process for a final semantic aligned generation. This leads us to question whether such a diffusion structure could be inductive to disentangled representation learning.

Originally, Variational Autoencoders (VAEs) are conceived as deep generative probabilistic models, primarily focusing on image generation tasks [Kingma and Welling, 2013]. The core idea behind VAEs is to model data distributions from the perspective of maximizing likelihood using variational inference. Subsequent research has revealed that VAEs possess the potential to learn disentangled representations with appropriate regularizations on simple datasets. To enhance disentanglement, a range of regularization losses have been proposed and integrated within the VAE framework [Higgins et al., 2017, Kim and Mnih, 2018, Kumar et al., 2017]. Similarly, GANs have incorporated regularizations to enable the learning of disentangled features [Chen et al., 2016, Lin et al., 2020, Zhu et al., 2021]. Despite significant progress, the disentanglement capabilities of these models remain less than satisfactory, and the disentangled representation learning is still very challenging. Locatello *et al*. demonstrate that relying solely on regularizations is insufficient for achieving disentanglement Locatello et al. [2019]. They emphasize the necessity of inductive biases on both the models and the data for effective disentanglement. A fresh perspective is eagerly anticipated to shed light on this field.

Recently, diffusion models have surfaced as compelling generative models known for their high sample quality [Yang et al., 2022a]. Drawing inspiration from the evolution of VAE-based disentanglement methods, we are intrigued by the question of whether diffusion models, also fundamentally designed as deep generative probabilistic models, possess the potential to learn disentangled representations. Obtaining a compact and disentangled representation for a given image from diffusion models is non-trivial. Diffusion Autoencoder (Diff-AE) [Preechakul et al., 2022] and PDAE [Zhang et al., 2022] move a step forward towards using diffusion models for representation learning by encoding the image into a feature vector, incorporating this into the diffusion generation process. However, these representations have not exhibited disentanglement characteristics. What inductive biases are essential for the learning of disentangled representations? Could we have a diffusion-based framework possessing such inductive biases?

Notably, in text-to-image generation, a conditional diffusion model integrates the '*disentangled*' text tokens through cross attention, demonstrating the ability to generate semantically aligned images [Rombach et al., 2022, Yang et al., 2022a, Hertz et al., 2022]. Interestingly, the observed cross-attention map reveals that different words have their corresponding spatial regions of high affinities, exhibiting strong semantic and spatial alignment as illustrated in Figure 1. These disentangled representations of 'word's could potentially contribute to a more streamlined generation process. Inspired by this, we wonder whether such diffusion structure with cross attention can act as an inductive bias to facilitate the disentangled representation learning.

In this paper, we endeavour to investigate this question and explore the potential of diffusion models in disentangled representation learning. We discover that the diffusion model with cross-attention can serve as a strong inductive bias to drive disentangled representation learning, even without any additional regularization. As illustrated in Figure 2 (a), we employ an encoder to transform an image into a set of concept tokens, which we treat as 'word' tokens, acting as the conditional input to the latent diffusion model with cross attention. Here, cross-attention bridges the interaction between the diffusion network and the image encoder. We refer to this scheme as EncDiff. EncDiff is powered by two valuable inductive biases, *i.e.*, information bottleneck in diffusion, and cross attention for fostering 'word' (concept token) and spatial alignment, contributing to the disentanglement. Experimental results on benchmark datasets demonstrate that EncDiff achieves excellent disentanglement performance, surpassing all the previous methods with elaborate designs. Comprehensive ablation studies show that the strong disentanglement capability is mainly attributed
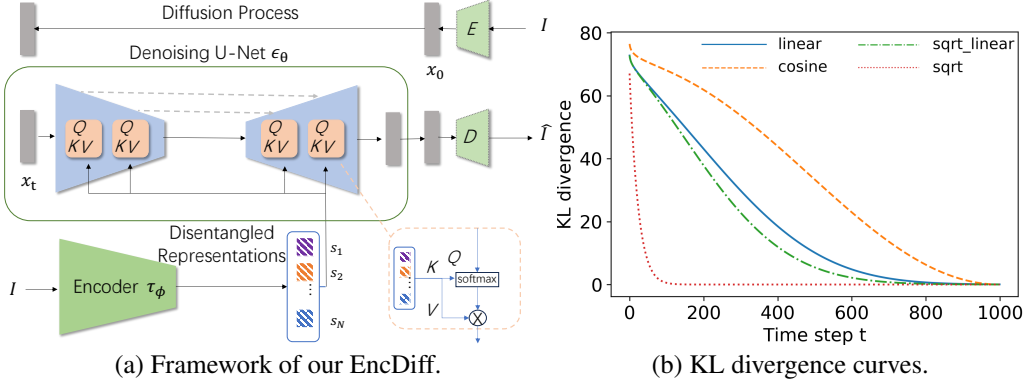
(a) Framework of our EncDiff.

(b) KL divergence curves.

Figure 2: (a) Illustration of our framework EncDiff. We employ an image encoder τ_ϕ to transform an image I into a set of disentangled representations, which we treat them as the conditional input to the latent diffusion model with cross attention. Here cross attention bridges the interaction between the diffusion network and the image encoder. For simplicity, we only briefly show the diffusion model which consists of an encoder E, a denoising U-Net and a decoder D that reconstructs the image from the latent x_t. (b) Information bottleneck reflected by KL divergence in reverse diffusion process. The KL divergence between the data distribution $q(x_{t-1}|x_t, x_0)$ and the Gaussian prior distribution $\mathcal{N}(0, \mathbf{I})$ under four different variance (β) schedules: cosine, linear, sqrt linear and sqrt. The results have been normalized by the number of dimensions.

to 1) the diffusion modelling and 2) the cross-attention interaction. Visualization analysis provides insights into the effectiveness of the disentangled representations.

We have four main contributions.

- We uncover that the diffusion model with cross-attention can serve as a strong inductive bias for enabling disentangled representation learning.
- We introduce a simple yet effective framework, EncDiff, powered by a latent diffusion model with cross attention and an ordinary image encoder, for disentangled representation learning.
- This framework inherently incorporates two valuable inductive biases: the information bottleneck in diffusion, and cross attention, fostering concept token and spatial alignment. We analyze that the diffusion process inherently possesses the time-varying information bottlenecks.
- Without additional regularization or specific designs, our framework achieves state-of-the-art disentanglement performance, even outperforming the latest methods with more complex designs.

We anticipate the new perspective will illuminate the field of disentanglement and inspire deeper investigations, paving the way for future sophisticated data analysis, understanding, and generation.

2 Related Work

Disentangled Representation Learning Disentangled Representation Learning endeavours to train a model proficient in disentangling the underlying factors of observed data [Bengio et al., 2013, Higgins et al., 2018, Wang et al., 2022]. A plethora of methods have been proposed to augment the generative models of VAEs and GANs, endowing them with disentanglement capability. These methods primarily rely on probability-based regularizations applied to the latent space. To improve disentanglement, most approaches focus on how to regularize the original VAE. For instance, this includes weighting the evidence lower bound (ELBO) as in β-VAE [Higgins et al., 2017], or introducing different terms to the ELBO, such as mutual information (InfoVAE [Zhao et al., 2017], InfoMax-VAE [Rezaabad and Vishwanath, 2020]), total correlation (Factor-VAE [Kim and Mnih, 2018]), and covariance (DIP-VAE [Kumar et al., 2017]). Locatello *et al.* [Locatello et al., 2019] demonstrate that relying solely on these regularizations is insufficient for achieving disentanglement. Inductive biases on both the models and the data are necessary. In this paper, we investigate the disentanglement capability of diffusion models and demonstrate that diffusion models with cross-attention can serve as a powerful inductive bias for disentanglement.

Diffusion Models Diffusion models have emerged as a powerful new family of deep probabilistic generative models [Yang et al., 2022a], surpassing VAEs and GANs for image generation and many

other tasks. Diffusion models progressively perturb data by injecting noise and then learn to reverse this process for the generation. A question arises as to whether diffusion models can effectively serve as disentangled representation learners. It is challenging to obtain a compact yet disentangled representation of an image from a diffusion model. Diff-AE [Preechakul et al., 2022] and PDAE [Zhang et al., 2022] investigate the possibility of using DPMs for representation learning, whereby an input image is autoencoded into a latent vector. However, these representations do not manifest disentangled characteristics. SlotDiffusion Wu et al. [2023] and LSD Jiang et al. [2023] integrate diffusion models into object-centric learning, where diffusion acts as a improved slot-to-image decoder, and slot attention is still the key for promoting object-centric learning. Moreover, they aim to learn object-wise representation but still cannot disentangle the factors/attributes of an object/a scene. Limited research has explored disentangled representation learning by leveraging diffusion models. InfoDiffusion [Wang et al., 2023] encourages the disentanglement of the latent feature of Diff-AE [Preechakul et al., 2022] by introducing mutual information and prior regularization, similar to InfoVAE [Zhao et al., 2017]. DisDiff [Yang et al., 2023b] employs a pre-trained diffusion model for disentangled feature learning. DisDiff adopts an encoder to learn the disentangled representations and a decoder to learn the sub-gradient field for each disentangled factor. It requires multiple decoders to predict these sub-gradient fields for all the factors and complex disentanglement losses, resulting in a costly and intricate process. Is it necessary to impose these complicated regularizations upon diffusion models? Does a strong inductive bias facilitating disentanglement already exist within diffusion models? In this paper, we endeavour to answer these questions and illustrate that a simple framework driven by a diffusion model without any additional regularization is capable of achieving superior disentanglement performance.

3 Method

We aim to investigate the potential of diffusion models in disentangled representation learning. We propose a simple yet effective framework, EncDiff, that exhibits strong disentanglement capabilities, even without additional regularizations. We analyze and identify two valuable inductive biases, *i.e.*, information bottleneck in diffusion, and the cross attention for fostering 'word' (concept token) and spatial alignment, thereby promoting disentanglement. We elaborate on the framework design in subsection 3.1 and the analysis in subsection 3.2, respectively.

3.1 Framework

Figure 2 (a) illustrates the flowchart. It consists of an image encoder that transforms an input image into a set of concept tokens and a diffusion model that serves as the decoder to reconstruct the image. Cross-attention is employed as the bridge for the diffusion network and the image encoder.

Image Encoder For a given input image I, the image encoder τ_ϕ aims to provide a set of concept tokens $\mathcal{S} = \{s_1, \cdots, s_N\}$, which act similarly to the word embeddings in the prompts for text-to-image generation in the latent diffusion models (LDMs) [Rombach et al., 2022]. Without loss of generality, we use an ordinary CNN network as the image encoder to obtain concept tokens. Following the design of the encoder in VAE [Kingma and Welling, 2013], we use a fully connected layer to transform the feature map into a feature vector. We treat each dimension of the encoded feature vector as a disentangled factor and map each factor to a vector (*i.e.*, concept token) by non-shared MLP layers (as illustrated by Figure 3).

Diffusion Model with Cross Attention We follow LDM [Rombach et al., 2022] to construct our diffusion model in the latent space, which demonstrates superior generation ability. LDM is one of the most popular diffusion models, proposing to conduct diffusion denoising in the latent space. To condition the concept tokens during image generation, cross-attention is used to map these tokens into the intermediate representations of the U-Net in the diffusion model. This is accomplished by using the cross-attention defined as $Attention(Q, K, V) = \text{softmax}\left(\frac{QK^T}{\sqrt{d}}\right) \cdot V$, where the spatial feature in the intermediate feature map in diffusion model serves as a query, the concept tokens act as keys and values.

End-to-End Training We conduct an end-to-end training of the encoder and the diffusion model, utilizing the optimization objective of reconstructing noise, which is a methodology aligned with that employed in LDM [Rombach et al., 2022].

3.2 Inductive Biases

We analyze that there are two crucial inductive biases in diffusion models: the information bottleneck in diffusion, and the cross-attention interaction. We analyze that the diffusion process inherently possesses the time-varying information bottlenecks.

3.2.1 Information Bottleneck in Diffusion

β-VAE [Higgins et al., 2017] and AnnealVAE [Burgess et al., 2018] utilize the original Kullback–Leibler (KL) divergence in VAEs to enhance the disentanglement capability, where the KL divergence constraint plays a role of an information bottleneck. Here, we analyze the presence of an information bottleneck mechanism that promotes the disentanglement in diffusion models. Without loss of generality, our analysis focuses on the diffusion model in image latent space Rombach et al. [2022]. The analysis also holds in pixel space.

Within the framework of the latent diffusion model, we add Gaussian noise to an image latent x_0 over T steps according to a variance schedule $\beta_1, \cdots, \beta_T$. This process yields a sequence of noisy samples $x_1, \cdots, x_T$,

$$q(x_t|x_{t-1}) := \mathcal{N}(x_t; \sqrt{1-\beta_t}x_{t-1}, \beta_t\mathbf{I}). \tag{1}$$

Let $\alpha_t = 1 - \beta_t$ and $\bar{\alpha}_t = \prod_{i=1}^{t} \alpha_t$. x_t can be obtained using the following equation [Ho et al., 2020, Yang et al., 2022a]:

$$x_t = \sqrt{\bar{\alpha}_t}x_0 + \sqrt{1-\bar{\alpha}_t}\epsilon, \tag{2}$$

where the noise ϵ is sampled from a Gaussian distribution $\mathcal{N}(0, \mathbf{I})$.

The diffusion model optimizes a network (*e.g.*, U-Net) ϵ_θ to predict the noise from the noisy input x_t and the conditioning input $\mathcal{S}$ (concept tokens), with the loss function defined as

$$\mathcal{L}_r = \mathbb{E}_{x_0,\epsilon,t}\|\epsilon_\theta(x_t, t, \mathcal{S}) - \epsilon\|. \tag{3}$$

Here, we omit the weighting terms of loss function for simplicity. The latent x_0 can be reconstructed based on the predicted noises.

Let's analyze the inherent information bottleneck at each time step t in the reverse diffusion process. In the reverse diffusion process, the reverse conditional distribution is tractable as Ho et al. [2020]:

$$q(x_t|x_{t-1}, x_0) = \mathcal{N}(x_{t-1}|\tilde{\mu}_t, \tilde{\beta}_t\mathbf{I}),$$
$$\text{where} \quad \tilde{\mu}_t = \frac{\sqrt{\bar{\alpha}_{t-1}}\beta_t}{1-\bar{\alpha}_t}x_0 + \frac{\sqrt{\alpha_t}(1-\bar{\alpha}_{t-1})}{1-\bar{\alpha}_t}x_t, \quad \tilde{\beta}_t = \frac{1-\bar{\alpha}_{t-1}}{1-\bar{\alpha}_t}\beta_t. \tag{4}$$

We formulate the Kullback-Leibler (KL) divergence C_t between $q(x_{t-1}|x_t, x_0)$ and the Gaussian prior distribution $p(x_{t-1}) = \mathcal{N}(0, \mathbf{I})$ at step $t-1$ as:

$$C_t = D_{KL}(q(x_{t-1}|x_t, x_0)\|p(x_{t-1})) = \frac{n}{2}(-\log\tilde{\beta}_t - 1 - \tilde{\beta}_t + \tilde{\mu}_t^T\tilde{\mu}_t/n), \tag{5}$$

where n denotes the number of dimension of signal x (*i.e.*, x_0, x_t, x_{t-1}).

In Figure 2 (b), we present a plot illustrating the KL divergence C_t under different variance (β) schedules, including linear, sqrt linear, cosine Nichol and Dhariwal [2021], Ho et al. [2020], and sqrt schedules Dhariwal and Nichol [2021], Rombach et al. [2022]. We can see that as the time step t decreases, the KL divergence C_t increases, indicating the information carried by x_{t-1} increases and leading to an increasingly looser information bottleneck over x_{t-1}. According to Burgess et al. [2018], Higgins et al. [2017], such a time-varying information bottleneck may play an important role in promoting disentanglement. Different variance (β) schedules results in different KL divergence curves. We found that these different variance schedules lead to different disentanglement performance (see Subsection 4.4).

Actually, optimizing the loss of conditional diffusion model as in (3) is equivalent to push the reverse conditional distribution $p_\theta(x_{t-1}|x_t, \mathcal{S})$ to approach $q(x_{t-1}|x_t, x_0)$ (see the explanation in Appendix B). By this means, the information bottlenecks $\tilde{C}_t = D_{KL}(p_\theta(x_{t-1}|x_t, \mathcal{S})\|p(x_{t-1}))$ over x_{t-1} tend to approach $C_t = D_{KL}(q(x_{t-1}|x_t, x_0)\|p(x_{t-1}))$ in training for all the time steps. According to theorem in Appendix C, the information bottleneck over latent x_{t-1} is transferred to the condition

$\mathcal{S}$ (i.e., concept tokens). Intuitively, this is because x_{t-1} is controlled by the concept tokens and the network parameters θ, as indicated by $p_\theta(x_{t-1}|x_t, \mathcal{S})$. The concept token representations $\mathcal{S}$ are learnable, and the information bottleneck is transferred to and imposed on $\mathcal{S}$. With time-varying information bottlenecks, the diffusion process encourages a range of different information capacities on $\mathcal{S}$ during the diffusion process, promoting the disentanglement of concept tokens.

Discussion The information bottleneck described above shares a certain similarity with the optimization objective in AnnealVAE [Burgess et al., 2018]. The minimizing objective of AnnealVAE is expressed as follows:

$$\mathcal{L}(\phi, \varphi) = - E_{q_\phi(z|x)}[\log p_\varphi(x|z)] + \gamma \|D_{KL}(q_\phi(z|x)\|p(z)) - C\|, \qquad (6)$$

where ϕ, φ are the parameters of the encoder and decoder; the latent representation and data are denoted as z, x, respectively. C is a handcrafted constant used to control the information bottleneck of the latent space. Different factors to be disentangled may contain different amounts of information. Instead of using a constant during training, AnnealVAE dynamically allocates larger amount of information (larger C) to the latent units as the training iteration increases. So that different factors can be learned at various training stages.

In diffusion models, where the KL divergence characterizes the information amount, we observe that the information amount varies in reverse diffusion steps, see Figure 2 (b).

3.2.2 Cross-Attention for Interaction

The information bottleneck sheds a light on disentangling, acting as an inductive bias for diffusion. However, using the information bottleneck still only has theoretical feasibility. Its effectiveness also relies on the structure design of diffusion model. We believe that the cross-attention design in conditional diffusion model is crucial for disentanglement, serving as another effective inductive bias.

Our objective is to train an encoder that obtains a set of concept tokens taking an image as input under the guidance of the diffusion model. We take the output of the encoder as the condition of the U-Net of diffusion model for image generation. We incorporate the concept tokens into diffusion model through cross-attention. Intuitively, a spatial position of an image is related to several concepts, *e.g.*, object color and shape in Shapes3D. Each spatial feature is composed of several related concept-based representations. Interestingly, cross-attention in the U-Net play a similar role, where each spatial feature servers as the query, and the learned concept tokens are used as the keys and values to refine the query. In subsection 4.4, we validate the necessity of the two inductive biases leading to disentanglement.

4 Experiments

4.1 Experimental Setup

Implementation Details We employ the popular diffusion structure of latent diffusion [Rombach et al., 2022] by default. Without loss of generality, following [Rombach et al., 2022], we use the VQ-reg to avoid arbitrarily high-variance latent spaces and sample images in 200 steps. We adopt the cosine as the variance (β) schedule in the diffusion model by default. By default, we use a CNN encoder for the image encoder to obtain a set of disentangled concept tokens. We use a CNN encoder similar to that used in [Yang et al., 2023b]. We denote our scheme as EncDiff.

Training Details During the training phase of EncDiff, we maintain a consistent batch size of 64 across all datasets. The learning rate is consistently set to 1×10^{-4}. We adopt the standard practice of employing an Exponential Moving Average (EMA) with a decay factor of 0.9999 for all model parameters. The training hyper-parameters follows DisDiff Yang et al. [2023b] and DisCo Ren et al. [2021]. For each concept token, we follow DisDiff Yang et al. [2023b] to use a 32 dimensional representation vector. We train EncDiff on a single Tesla V100 16G GPU. A model takes about 1 day for training.

Datasets To evaluate the disentanglement performance, we utilize the commonly used benchmark datasets: Shapes3D [Kim and Mnih, 2018], MPI3D [Gondal et al., 2019] and Cars3D [Reed et al., 2015]. Shapes3D [Kim and Mnih, 2018] consists of a collection of 3D shapes. MPI3D is a dataset of 3D objects created in a controlled setting. Cars3D is a dataset consisting of 3D-rendered cars. For

6

Table 1: Comparisons of disentanglement on the FactorVAE score and DCI disentanglement metrics (mean $\pm$ std, higher is better). EncDiff outperforms the state-of-the-art methods with a large margin except on Cars3D.

Method	Cars3D		Shapes3D		MPI3D	
	FactorVAE score↑	DCI↑	FactorVAE score↑	DCI↑	FactorVAE score↑	DCI↑
VAE-based:						
FactorVAE Kim and Mnih [2018]	0.906 ± 0.052	0.161 ± 0.019	0.840 ± 0.066	0.611 ± 0.082	0.152 ± 0.025	0.240 ± 0.051
β-TCVAE Chen et al. [2018]	0.855 ± 0.082	0.140 ± 0.019	0.873 ± 0.074	0.613 ± 0.114	0.179 ± 0.017	0.237 ± 0.056
GAN-based:						
InfoGAN-CR Lin et al. [2020]	0.411 ± 0.013	0.020 ± 0.011	0.587 ± 0.058	0.478 ± 0.055	0.439 ± 0.061	0.241 ± 0.075
Pre-trained GAN-based:						
LD [Voynov and Babenko, 2020]	0.852 ± 0.039	0.216 ± 0.072	0.805 ± 0.064	0.380 ± 0.062	0.391 ± 0.039	0.196 ± 0.038
GS [Härkönen et al., 2020]	0.932 ± 0.018	0.209 ± 0.031	0.788 ± 0.091	0.284 ± 0.034	0.465 ± 0.036	0.229 ± 0.042
DisCo Ren et al. [2021]	0.855 ± 0.074	0.271 ± 0.037	0.877 ± 0.031	0.708 ± 0.048	0.371 ± 0.030	0.292 ± 0.024
Diffusion-based:						
DisDiff Yang et al. [2023b]	$\mathbf{0.976} \pm 0.018$	0.232 ± 0.019	0.902 ± 0.043	0.723 ± 0.013	0.617 ± 0.070	0.337 ± 0.057
EncDiff (Ours)	0.773 ± 0.060	$\mathbf{0.279} \pm 0.022$	$\mathbf{0.999} \pm 0.000$	$\mathbf{0.969} \pm 0.030$	$\mathbf{0.872} \pm 0.049$	$\mathbf{0.685} \pm 0.044$

real-world data, we conduct our experiments using CelebA, a dataset of celebrity faces with attributes. Our experiments are carried out at a 64×64 image resolution, consistent with previous studies [Kim and Mnih, 2018, Chen et al., 2018, Ren et al., 2021, Yang et al., 2023b].

Baselines & Metrics We compare the performance of our method with VAE-based, GAN-based, and diffusion-based methods, following the experimental protocol as in DisCo [Ren et al., 2021]. The VAE-based models we use for comparison are FactorVAE [Kim and Mnih, 2018] and β-TCVAE [Chen et al., 2018], while the GAN-based baselines include InfoGAN-CR [Lin et al., 2020], GANspace (GS) [Härkönen et al., 2020], LatentDiscovery (LD) [Voynov and Babenko, 2020] and DisCo [Ren et al., 2021]. Each method utilizes scalar-valued representations. DisDiff [Yang et al., 2023b] uses vector-valued representations. EncDiff has two kinds of representations simultaneously. We focus on the scalar-valued in the main paper. We follow DisDiff to set N to 20. For these vector-valued representations, we follow Du et al. [2021], Yang et al. [2023b,a] to perform PCA as a post-processing on the representation before evaluation. To assess the potential variability in performance due to random seed selection, we have fifteen runs for each method for reliable evaluation, reporting the mean and variance. Regarding evaluation metrics, we adopt two representative metrics, the FactorVAE score [Kim and Mnih, 2018] and the DCI [Eastwood and Williams, 2018].

4.2 Comparison with the State-of-the-Arts

We compare the disentanglement ability of our EncDiff with the state-of-the-art methods. Table 1 shows quantitative comparison results of disentanglement under different metrics. We can see that EncDiff achieves the best performance on all the datasets except Cars3D, showcasing the model's superior disentanglement ability. EncDiff achieves superior performance by leveraging the strong inductive bias from the diffusion model with cross-attention without using any additional regularization losses. EncDiff also outperforms InfoDiffusion [Wang et al., 2023] and DisDiff [Yang et al., 2023b] by a significant marginal, even though DisDiff uses complex disentanglement loss and inference the decoder multiple times for prediction sub-gradient fields. On the Cars3D dataset, the quantitative evaluation is not so reliable because some factors, such as color and shape, are not included in the labels. From the visualization in Figure 6 of Appendix E, we can see that EncDiff achieves superior disentanglement compared to DisDiff despite the lower FactorVAE score.

In addition, our EncDiff achieves superior reconstruction quality (see Appendix G for more details).

4.3 Visualization

Visualization Analysis on the Disentanglement We qualitatively examine the disentanglement properties of our proposed method. We interchange the concept tokens (factors) of the learned representation of two distinct images and observe the generated images conditioned on these exchanged representations. For illustration purposes, we focus on the widely used Shapes3D dataset from the disentanglement literature and show the results in Figure 4. We can see that our EncDiff successfully
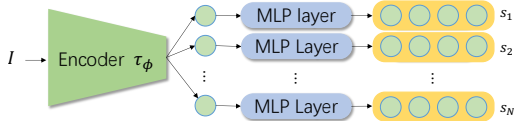
Figure 3: Illustration of the encoder τ_ϕ, which transforms an image into a feature vector of dimension N, with each dimension (scalar) encoding a disentangled factor. We then use non-shared three-layer MLP layers to map each scalar into a vector (concept token). The concept tokens will be treated as the conditional input to the latent diffusion model with cross attention.

Table 2: Comparisons of disentanglement performance and generation quality in terms of TAD and FID metrics (mean $\pm$ std) on real-world dataset CelebA. EncDiff achieves the state-of-the-art performance on both aspects compared to all baselines.

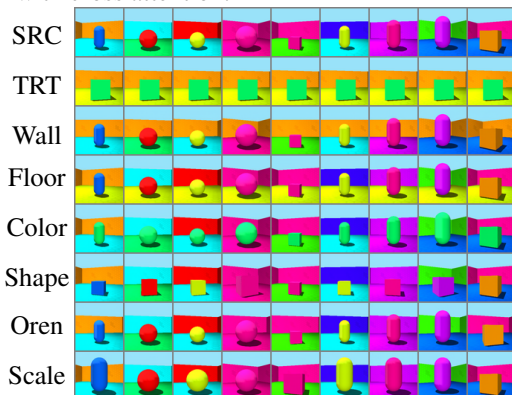| Model	TAD $\uparrow$	FID $\downarrow$
β-VAE Higgins et al. [2017]	0.088 ± 0.043	99.8 ± 2.4
InfoVAE Zhao et al. [2017]	0.000 ± 0.000	77.8 ± 1.6
Diff-AE Preechakul et al. [2022]	0.155 ± 0.010	22.7 ± 2.1
InfoDiffusion Wang et al. [2023]	0.299 ± 0.006	23.6 ± 1.3
DisDiff Yang et al. [2023b]	0.305 ± 0.010	18.2 ± 2.1
EncDiff	$\mathbf{0.638 \pm 0.008}$	$\mathbf{14.8 \pm 2.3}$

Figure 4: The qualitative results on Shapes3D. The source (SRC) images provide the representations of the generated image. The target (TRT) image provides the representation for swapping. Other images are generated by swapping the representation of the corresponding factor. For Shapes3D, the learned factors on Shapes3D are wall color (Wall), floor color (Floor), object color (Color), and object shape (Shape), orientation (Orien), scale. See Appendix E for more visualizations.

isolates factors. Notably, in comparison to VAE-based methods, EncDiff delivers superior image quality quantitatively (please refer to Appendix H).

Visualization of Learned Cross-Attention Maps As mentioned in Section 1, our model draws inspiration from the alignment between 'word' tokens (disentangled representations) and spatial features. The alignment is demonstrated by the learned cross-attention maps. We verify whether our learned concept tokens present the disentangled characteristics by visualizing the alignment of concept tokens with spatial positions through cross-attention maps. As depicted in Figure 5, the results of our model exhibit exemplary alignment between concept tokens and spatial positions. Distinct concept tokens are associated with varying attended spatial regions, corresponding to different semantics that are comprehensible by humans, such as the region of "Wall" and "Floor" for the images from Shapes3D.

4.4 Ablation Study

In our framework, in order to analyze and understand the key factors contributing to the advancement of disentangled representation learning, we conduct ablation studies covering three aspects in the design: 1) whether to use diffusion as the decoder; 2) whether to use cross-attention as the bridge for interaction; 3) The influence of different variance (β) schedules. We conduct these ablation studies on the Shapes3D dataset. Please see Appendix H for more ablation studies.

Using Diffusion as Decoder or Not To validate whether the use of a diffusion model as an inductive bias for disentangled representation learning is crucial, we employ a network structure similar to the U-Net in our used diffusion model as the decoder, utilizing reconstruction l_2 loss is used to optimize the entire network. Specifically, we remove the encoder part of the U-Net and the skip connection between it and the decoder part of the U-Net. We then feed the U-Net decoder with a
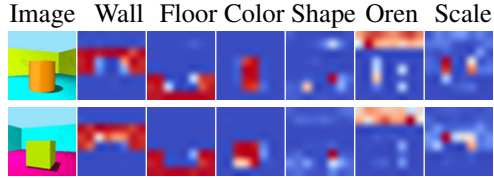
8

Figure 5: Visualization of the cross-attention maps on Shapes3D. The first column shows the original image while the other columns show the attention masks for different concept tokens. See Appendix F for more visualizations.

randomly initialized learnable spatial tensor to maintain the structure of the decoder U-Net. Similarly to EncDiff, the encoded disentangled representations are input to the decoder through cross-attention (CA). We refer to this scheme as *EncDec w/o Diff*. Table 3 shows the results. The performance of *EncDiff* with diffusion significantly outperforms *EncDec w/o Diff* by 0.46 and 0.79 in terms of FactorVAE score and DCI, respectively. This indicates that inductive bias from diffusion modelling is crucial for achieving effective disentanglement.

Table 3: Influence of the two inductive biases. For *EncDec w/o Diff*, we replace the diffusion model with a decoder while cross-attention is preserved. For *EncDiff w/ AdaGN*, we replace the cross-attention with AdaGN.

Method	FactorVAE score↑	DCI↑
EncDec w/o Diff	0.537 ± 0.074	0.178 ± 0.050
EncDiff w/ AdaGN	0.911 ± 0.101	0.637 ± 0.068
EncDiff	$\mathbf{0.999} \pm 0.000$	$\mathbf{0.969} \pm 0.030$

Table 4: Ablation study on the influence of the variance (β) schedule. We use four kinds of variance schedules: sqrt, cosine, linear, and sqrt linear.

Method	FactorVAE score↑	DCI↑
EncDiff w/sqrt	0.997 ± 0.011	0.950 ± 0.041
EncDiff w/sqrt linear	0.988 ± 0.026	0.924 ± 0.050
EncDiff w/linear	0.999 ± 0.002	0.930 ± 0.045
EncDiff w/cosine	$\mathbf{0.999} \pm 0.001$	$\mathbf{0.969} \pm 0.030$

Using Cross-Attention for Interaction To incorporate the image representation to the diffusion model as a condition, we use cross-attention by treating each disentangled representation as a conditional token (similar to the use of 'word' token in text-to-image generation in stable diffusion model [Rombach et al., 2022]). As an alternative, similar to that in Diff-AE [Preechakul et al., 2022] and InfoDiffusion [Wang et al., 2023], we use adaptive group normalization (AdaGN) to incorporate the representation vector (by concatenating the concept tokens) to modulate the spatial features. We name this scheme as *EncDiff w/ AdaGN*. Table 3 presents the results. We can see that *EncDiff w/ AdaGN* is inferior to *EncDiff*, with a significant decrease of 0.33 in terms of DCI. Cross-attention facilitates the alignment of each concept token with the corresponding spatial features, akin to the alignment of the 'word' token to spatial features in the text-to-image generation. In contrast, AdaGN did not efficiently promote disentanglement.

Influence of Different Variance (β) Schedules We investigate the influence of the different variance (β) schedules, including including linear, sqrt linear, cosine Nichol and Dhariwal [2021], Ho et al. [2020], sqrt schedules Dhariwal and Nichol [2021], Rombach et al. [2022], on the disentanglement performance. From Table 4, we can see that distinct schedules result in different performance, demonstrating the influence on disentanglement of different information bottleneck schedules. Note that the FactorVAE scores are all very high and cannot well reflect the performance. We prefer to use DCI metric here for evaluation. We can see that the cosine schedule performs the best and we adopt it by default. The linear schedule approaches that of the sqrt linear in terms of the curve shape, please see Figure 2 (b) and achieves the similar performance in terms of DCI.

Scalar-valued vs. Vector-valued Manners We treat each dimension of the encoded feature vector as a disentangled factor, followed by a mapping to concept token (vector) for each factor. Another design alternative is to directly split the feature vector into N chunks, with each chunk being a concept token, similar to DisDiff [Yang et al., 2023b]. We name this vector-valued design and refer to it by DisDiff-V. Table 5 shows that EncDiff outperforms EncDiff-V obviously. The intermediate scalar design in EncDiff may serve a bottleneck role and contribute to the disentanglement.

4.5 Computational Complexity

We compare the computational complexity of Diff-AE Preechakul et al. [2022], DisDiff [Yang et al., 2023b], and our EncDiff in terms of the parameters (Params.), floating-point operations (FLOPs),

Table 5: Ablation study on the two design alternatives on obtaining the token representations.

Method	FactorVAE score ↑	DCI↑
EncDiff-V	0.999 ± 0.000	0.900 ± 0.045
EncDiff	$\mathbf{0.999} \pm 0.001$	$\mathbf{0.969} \pm 0.030$

Table 6: Computational complexity comparison.

Method	Params.↓ (M)	FLOPs↓ (M)	Time↓ (s)
Diff-AE Preechakul et al. [2022]	67.8	3955.1	31.0
DisDiff Yang et al. [2023b]	57.1	5815.8	35.3
EncDiff	42.3	2898.5	11.8

and inference time (seconds/sample) for sampling an image. As shown in Table 6, our EncDiff demonstrates much higher computational efficiency than Diff-AE and DisDiff.

5 Limitations

Our method operates in a fully unsupervised manner and exhibits strong disentanglement capability on simple datasets. Similar to other disentanglement-based methods [Higgins et al., 2017, Kim and Mnih, 2018, Chen et al., 2016, Lin et al., 2020, Yang et al., 2021], obtaining satisfactory performance on complex data remains a challenge. As a diffusion-based method, the generation speed of EncDiff is faster than DisDiff [Yang et al., 2023b]. However, it is still slower compared to VAE-based and GAN-based methods. More effective sampling strategies, as employed in DPM-based methods, could be utilized for accelerating in the future.

6 Conclusion

This paper unveils a fresh viewpoint, demonstrating that diffusion models with cross-attention can serve as a strong inductive bias to foster disentangled representation learning. Within our framework EncDiff, we reveal that the diffusion model structure with cross-attention can drive an image encoder to learn superior disentangled representations, even without any regularization. Our comprehensive ablation studies demonstrate that the strong capability is mainly attributed to diffusion modelling and cross-attention interaction. This work will inspire further investigations on diffusion for disentanglement, paving the way for sophisticated data analysis, understanding, and generation.

References

Yoshua Bengio, Aaron C. Courville, and Pascal Vincent. Representation learning: A review and new perspectives. *PAMI*, 2013.

Christopher P Burgess, Irina Higgins, Arka Pal, Loic Matthey, Nick Watters, Guillaume Desjardins, and Alexander Lerchner. Understanding disentangling in beta-vae. *arXiv:1804.03599*, 2018.

Jaehoon Cha and Jeyan Thiyagalingam. Orthogonality-enforced latent space in autoencoders: An approach to learning disentangled representations. In *International Conference on Machine Learning*, pages 3913–3948. PMLR, 2023.

Ricky TQ Chen, Xuechen Li, Roger B Grosse, and David K Duvenaud. Isolating sources of disentanglement in variational autoencoders. In *NeurPIS*, 2018.

Xi Chen, Yan Duan, Rein Houthooft, John Schulman, Ilya Sutskever, and Pieter Abbeel. Info-GAN: Interpretable representation learning by information maximizing generative adversarial nets. *Advances in neural information processing systems*, 29, 2016.

Prafulla Dhariwal and Alexander Nichol. Diffusion models beat gans on image synthesis. *Advances in Neural Information Processing Systems*, 34:8780–8794, 2021.

Yilun Du, Shuang Li, Yash Sharma, Josh Tenenbaum, and Igor Mordatch. Unsupervised learning of compositional energy concepts. In *Advances in Neural Information Processing Systems*, volume 34, 2021.

Cian Eastwood and Christopher K. I. Williams. A framework for the quantitative evaluation of disentangled representations. In *ICLR*, 2018.

Marco Fumero, Florian Wenzel, Luca Zancato, Alessandro Achille, Emanuele Rodolà, Stefano Soatto, Bernhard Schölkopf, and Francesco Locatello. Leveraging sparse and shared feature activations for disentangled representation learning. *Advances in Neural Information Processing Systems*, 36, 2023.

Muhammad Waleed Gondal, Manuel Wuthrich, Djordje Miladinovic, Francesco Locatello, Martin Breidt, Valentin Volchkov, Joel Akpo, Olivier Bachem, Bernhard Schölkopf, and Stefan Bauer. On the transfer of inductive bias from simulation to the real world: a new disentanglement dataset. In *NeurIPS*, 2019.

Erik Härkönen, Aaron Hertzmann, Jaakko Lehtinen, and Sylvain Paris. Ganspace: Discovering interpretable GAN controls. In *NeurIPS*, 2020.

Amir Hertz, Ron Mokady, Jay Tenenbaum, Kfir Aberman, Yael Pritch, and Daniel Cohen-Or. Prompt-to-prompt image editing with cross attention control. *arXiv preprint arXiv:2208.01626*, 2022.

Irina Higgins, Loïc Matthey, Arka Pal, Christopher Burgess, Xavier Glorot, Matthew Botvinick, Shakir Mohamed, and Alexander Lerchner. beta-vae: Learning basic visual concepts with a constrained variational framework. In *ICLR*, 2017.

Irina Higgins, David Amos, David Pfau, Sebastien Racaniere, Loic Matthey, Danilo Rezende, and Alexander Lerchner. Towards a definition of disentangled representations. *arXiv preprint arXiv:1812.02230*, 2018.

Jonathan Ho, Ajay Jain, and Pieter Abbeel. Denoising diffusion probabilistic models. *Advances in neural information processing systems*, 33:6840–6851, 2020.

Jindong Jiang, Fei Deng, Gautam Singh, and Sungjin Ahn. Object-centric slot diffusion. *Advances in Neural Information Processing Systems*, 2023.

Hyunjik Kim and Andriy Mnih. Disentangling by factorising. In *ICML*, 2018.

Diederik P Kingma and Max Welling. Auto-encoding variational bayes. *arXiv preprint arXiv:1312.6114*, 2013.

Abhishek Kumar, Prasanna Sattigeri, and Avinash Balakrishnan. Variational inference of disentangled latent concepts from unlabeled observations. *arXiv preprint arXiv:1711.00848*, 2017.

Felix Leeb, Giulia Lanzillotta, Yashas Annadani, Michel Besserve, Stefan Bauer, and Bernhard Schölkopf. Structure by architecture: Structured representations without regularization. In *The Eleventh International Conference on Learning Representations*, 2022.

Zinan Lin, Kiran Thekumparampil, Giulia Fanti, and Sewoong Oh. Infogan-cr and modelcentrality: Self-supervised model training and selection for disentangling gans. In *ICML*, 2020.

Francesco Locatello, Stefan Bauer, Mario Lucic, Gunnar Raetsch, Sylvain Gelly, Bernhard Schölkopf, and Olivier Bachem. Challenging common assumptions in the unsupervised learning of disentangled representations. In *international conference on machine learning*, pages 4114–4124. PMLR, 2019.

Alexander Quinn Nichol and Prafulla Dhariwal. Improved denoising diffusion probabilistic models. In *International Conference on Machine Learning*, pages 8162–8171. PMLR, 2021.

Konpat Preechakul, Nattanat Chatthee, Suttisak Wizadwongsa, and Supasorn Suwajanakorn. Diffusion autoencoders: Toward a meaningful and decodable representation. In *IEEE Conference on Computer Vision and Pattern Recognition (CVPR)*, 2022.

Scott E. Reed, Yi Zhang, Yuting Zhang, and Honglak Lee. Deep visual analogy-making. In *NeurIPS*, 2015.

Xuanchi Ren, Tao Yang, Yuwang Wang, and Wenjun Zeng. Learning disentangled representation by exploiting pretrained generative models: A contrastive learning view. In *International Conference on Learning Representations*, 2021.

Ali Lotfi Rezaabad and Sriram Vishwanath. Learning representations by maximizing mutual information in variational autoencoders. In *IEEE International Symposium on Information Theory (ISIT)*, pages 2729–2734, 2020.

Robin Rombach, Andreas Blattmann, Dominik Lorenz, Patrick Esser, and Björn Ommer. High-resolution image synthesis with latent diffusion models. In *IEEE/CVF conference on computer vision and pattern recognition*, pages 10684–10695, 2022.

Andrey Voynov and Artem Babenko. Unsupervised discovery of interpretable directions in the GAN latent space. In *ICML*, 2020.

Xin Wang, Hong Chen, Si'ao Tang, Zihao Wu, and Wenwu Zhu. Disentangled representation learning. *arXiv preprint arXiv:2211.11695*, 2022.

Yingheng Wang, Yair Schiff, Aaron Gokaslan, Weishen Pan, Fei Wang, Christopher De Sa, and Volodymyr Kuleshov. Infodiffusion: Representation learning using information maximizing diffusion models. *International conference on machine learning*, 2023.

Ziyi Wu, Jingyu Hu, Wuyue Lu, Igor Gilitschenski, and Animesh Garg. Slotdiffusion: Object-centric generative modeling with diffusion models. *Advances in Neural Information Processing Systems*, 2023.

Ling Yang, Zhilong Zhang, Yang Song, Shenda Hong, Runsheng Xu, Yue Zhao, Wentao Zhang, Bin Cui, and Ming-Hsuan Yang. Diffusion models: A comprehensive survey of methods and applications. *ACM Computing Surveys*, 2022a.

Tao Yang, Xuanchi Ren, Yuwang Wang, Wenjun Zeng, and Nanning Zheng. Towards building a group-based unsupervised representation disentanglement framework. In *International Conference on Learning Representations*, 2021.

Tao Yang, Yuwang Wang, Yan Lu, and Nanning Zheng. Visual concepts tokenization. *Advances in Neural Information Processing Systems*, 35:31571–31582, 2022b.

Tao Yang, Yuwang Wang, Cuiling Lan, Yan Lu, and Nanning Zheng. Vector-based representation is the key: A study on disentanglement and compositional generalization. *arXiv preprint arXiv:2305.18063*, 2023a.

Tao Yang, Yuwang Wang, Yan Lv, and Nanning Zh. Disdiff: Unsupervised disentanglement of diffusion probabilistic models. *Advances in Neural Information Processing Systems*, 2023b.

Tao Yang, Yuwang Wang, Yan Lv, and Nanning Zheng. Disdiff: Unsupervised disentanglement of diffusion probabilistic models, january 2023b. *Advances in Neural Information Processing Systems*, 2023c.

Zijian Zhang, Zhou Zhao, and Zhijie Lin. Unsupervised representation learning from pre-trained diffusion probabilistic models. *NeurIPS*, 2022.

Shengjia Zhao, Jiaming Song, and Stefano Ermon. InfoVAE: Information maximizing variational autoencoders. *arXiv preprint arXiv:1706.02262*, 2017.

Xinqi Zhu, Chang Xu, and Dacheng Tao. Where and what? examining interpretable disentangled representations. In *IEEE Conference on Computer Vision and Pattern Recognition*, pages 5861–5870, 2021.

A Impact Statements

This paper presents work whose goal is to advance the field of disentanglement learning. Our research is designed to be a positive force for innovation purpose. Viewed from a societal lens, the potential negative impacts is the malicious use of the models. This highlights the critical necessity of incorporating ethical considerations in the utilization of our method for responsible AI.

B Optimization of the Reverse Conditional Probability $p_\theta(x_{t-1}|x_t, \mathcal{S})$

Two distinct approaches exist for decomposing the loss function, Variational Lower Bound(VLB), of the diffusion model. The derivations presented herein closely follow the methodology outlined by Ho et al. Ho et al. [2020]. Without loss of generality, we could incorporate the conditional input denoted by $\mathcal{S}$ to the diffusion.

For the first decomposition alternative, we can derive the following equations:

$$
\begin{aligned}
\mathcal{L} &= \mathbb{E}_q \left[-\log \frac{p_\theta(x_{0:T}|\mathcal{S})}{q(x_{1:T}|x_0)} \right] \\
&= \mathbb{E}_q \left[\log \frac{\Pi_{t=1}^T q(x_t|x_{t-1})}{p(x_T)\Pi_{t=1}^T p_\theta(x_{t-1}|x_t, \mathcal{S})} \right] \\
&= \mathbb{E}_q \left[-\log p(x_T) + \Sigma_{t\geq 1} \log \frac{q(x_t|x_{t-1})}{p_\theta(x_{t-1}|x_t, \mathcal{S})} \right] \\
&= \mathbb{E}_q \left[-\log p(x_T) - \Sigma_{t>1} \log \frac{p_\theta(x_{t-1}|x_t, \mathcal{S})}{q(x_t|x_{t-1})} - \log \frac{p_\theta(x_0|x_1)}{q(x_1|x_0)} \right].
\end{aligned}
\tag{7}
$$

By applying Bayes' Rule and the Markov property of the diffusion process, we conclude that

$$
q(x_{t-1}|x_t, x_0) = \frac{q(x_t|x_{t-1}, x_0)q(x_{t-1}|x_0)}{q(x_t|x_0)} = \frac{q(x_t|x_{t-1})q(x_{t-1}|x_0)}{q(x_t|x_0)}.
\tag{8}
$$

This leads to

$$
\begin{aligned}
\mathcal{L} &= \mathbb{E}_q \left[-\log p(x_T) - \Sigma_{t>1} \log \frac{p_\theta(x_{t-1}|x_t, \mathcal{S})}{q(x_{t-1}|x_t, x_0)} \frac{q(x_{t-1}|x_0)}{q(x_t|x_0)} - \log \frac{p_\theta(x_0|x_1)}{q(x_1|x_0)} \right] \\
&= \mathbb{E}_q \left[-\log \frac{p(x_T)}{q(x_T|x_0)} - \Sigma_{t>1} \log \frac{p_\theta(x_{t-1}|x_t, \mathcal{S})}{q(x_{t-1}|x_t, x_0)} - \log p_\theta(x_0|x_1) \right] \\
&= \mathbb{E}_q \left[D_{KL}(q(x_T|x_0)||p(x_T)) + \Sigma_{t>1} D_{KL}(q(x_{t-1}|x_t, x_0)||p_\theta(x_{t-1}|x_t, \mathcal{S})) - \log p_\theta(x_0|x_1) \right].
\end{aligned}
\tag{9}
$$

For the second alternative, the loss function is derived to be $\mathbb{E}_{x_0, \epsilon, t}\|\epsilon_\theta(x_t, t, \mathcal{S}) - \epsilon\|$ Ho et al. [2020].

The optimization of conditional diffusion model by predicting the noises through minimizing $\mathbb{E}_{x_0, \epsilon, t}\|\epsilon_\theta(x_t, t, \mathcal{S}) - \epsilon\|$ is thus equivalent to minimizing the second term of (9), *i.e.*, $\Sigma_{t>1} D_{KL}(q(x_{t-1}|x_t, x_0)||p_\theta(x_{t-1}|x_t, \mathcal{S}))$, which pushes the reverse conditional probability $p_\theta(x_{t-1}|x_t, \mathcal{S})$ to approach $q(x_{t-1}|x_t, x_0)$.

C The Transfer of Information Bottleneck

Theorem C.1. *The Kullback-Leibler divergence is invariant under a differentiable mapping f, i.e .*

$$
D_{KL}(p(x)|q(x)) = D_{KL}(p(S)|q(S))
$$

where $x = f(S)$ is a differentiable function between x and S and $p(x)$ and $q(x)$ are the probability density functions of the probability distributions P and Q, respectively.

Proof: The Kullback-Leibler divergence (KL divergence) is defined as

$$
D_{KL}(p(x)|q(x)) = \int p(x) \log \frac{p(x)}{q(x)} dx
$$

According to the change of variable theorem, we have

$$
\begin{aligned}
p(x) &= p(f(x))|f'(x)| = p(S)|f'(x)| \\
q(x) &= q(f(x))|f'(x)| = q(S)|f'(x)|
\end{aligned}
\tag{10}
$$

where $|f'(x)|$ denotes the Jacobian of $f(x)$, $p(S)$ is the corresponding distribution of $p(x)$ under the mapping f. $q(S)$ is the corresponding distribution of $q(x)$ under the mapping f. Combine the two equations, we have

$$
D_{KL}(p(x)|q(x)) = \int p(f(x))|f'(x)| \log \frac{p(f(x))|f'(x)|}{q(f(x))|f'(x)|} dx = \int p(f(x)) \log \frac{p(f(x))}{q(f(x))} |f'(x)| dx.
\tag{11}
$$

Considering the property of integral that for $S = f(x)$ we have $dS = |f'(x)|dx$. We then have the following:

$$
D_{KL}(p(x)|q(x)) = \int p(S) \log \frac{p(S)}{q(S)} dS = D_{KL}(p(S)|q(S)).
\tag{12}
$$

This indicates that the information bottleneck on x is transferable to the input S of the function.

D   Implementation Details

For our EncDiff (scalar-valued), following the approach of Leeb et al. [2022], each dimension of the encoded feature vector is treated as a disentangled factor. Each factor is then mapped to a vector (i.e., concept token) using non-shared MLP layers, as illustrated in Figure 3. For vector-valued EncDiff (EncDiff-V), inspired by DisDiff [Yang et al., 2023b], we partition the feature vector into N (e.g., 20) chunks, referred to as concept tokens, to encode different factors.

Image Encoder Architecture To ensure an equitable comparison, we employ the encoder architecture, consistent with DisCo Ren et al. [2021] and DisDiff Yang et al. [2023b]. The encoder specifications are detailed in Table 7.

Table 7: Encoder architecture used in EncDiff.

Conv $7 \times 7 \times 3 \times 64$, stride $= 1$
ReLu
Conv $4 \times 4 \times 64 \times 128$, stride $= 2$
ReLu
Conv $4 \times 4 \times 128 \times 256$, stride $= 2$
ReLu
Conv $4 \times 4 \times 256 \times 256$, stride $= 2$
ReLu
Conv $4 \times 4 \times 256 \times 256$, stride $= 2$
ReLu
FC 4096×256
ReLu
FC 256×256
ReLu
FC $256 \times K$

Diffusion U-Net Architecture The diffusion architecture adheres to the design principles of latent diffusion Rombach et al. [2022] and DisDiff Zhang et al. [2022]. Table 8 provides a detailed overview of the network structure, similar to the structure of Latent Diffusion Probabilistic Model.

We pretrain VQ-VAE in diffusion. Then the diffusion network and our image encoder are jointly trained.

E   More Visualizations

We present qualitative results for Cars3D in Figure 6. Notably, on the synthetic dataset Cars3D, EncDiff demonstrates the acquisition of disentangled representations, presenting better disentanglement ability than DisDiff Yang et al. [2023b]). We can see that our EncDiff can capture the factors of

Table 8: U-Net architecture used in EncDiff.

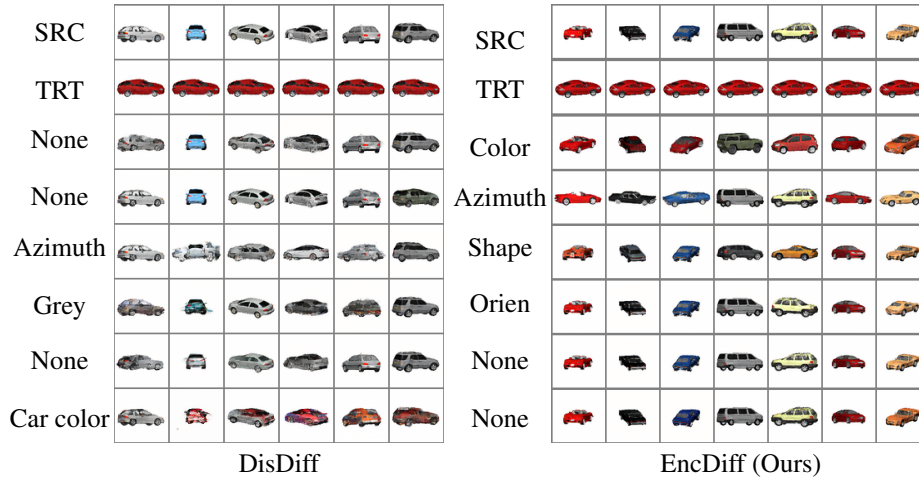| Parameters	Shapes3D / Cars3D/ MPI3D /CelebA
Base channels	16
Channel multipliers	[1, 2, 4, 4]
Attention resolutions	[1, 2, 4]
Attention heads num	8
Model channels	64
Dropout	0.1
Images trained	0.48M / 0.28M / 1.03M
β scheduler	Cosine (Sqrt/Sqrt linear/Linear)
Training T	1000
Diffusion loss	MSE with noise prediction ϵ

Figure 6: The qualitative comparison on Cars3D. The source (SRC) images provide the representations of the generated image. The target (TRT) image provides the representation for swapping. Other images are generated by swapping the representation of the corresponding factor. "Orien" refers to Orientation. We can see that our EncDiff can capture the factors of "Color", "Azimuth", and "Shape" while DisDiff failed to capturing them.

"Color", "Azimuth", and "Shape" while DisDiff failed to capturing them. Furthermore, we include three rows of images demonstrating the manipulation of representations lacking informative content, denoted as "None".

We present the qualitative outcomes for MPI3D in Figure 7. Remarkably, on the challenging disentanglement dataset MPI3D, EncDiff showcases its ability to obtain disentangled representations.

F   More Visualizations on Attention Maps

We showcase the visualization of attention maps for our model's disentangled representations on the Cars3D dataset, as depicted in Figure 8. Similar to EncDiff, the attention maps provide insights into the acquisition of disentangled representations in the synthetic setting of Cars3D. Notably, our attention maps reveal distinct alignments between concept tokens and spatial features, demonstrating the disentangled characteristics learned by our model.

For the MPI3D dataset, Figure 8 demonstrate the qualitative outcomes of attention map visualization. In this challenging disentanglement scenario, EncDiff excels in acquiring disentangled representations. The attention maps further illustrate the alignment between concept tokens and spatial positions, affirming the model's ability to disentangle complex features in MPI3D.
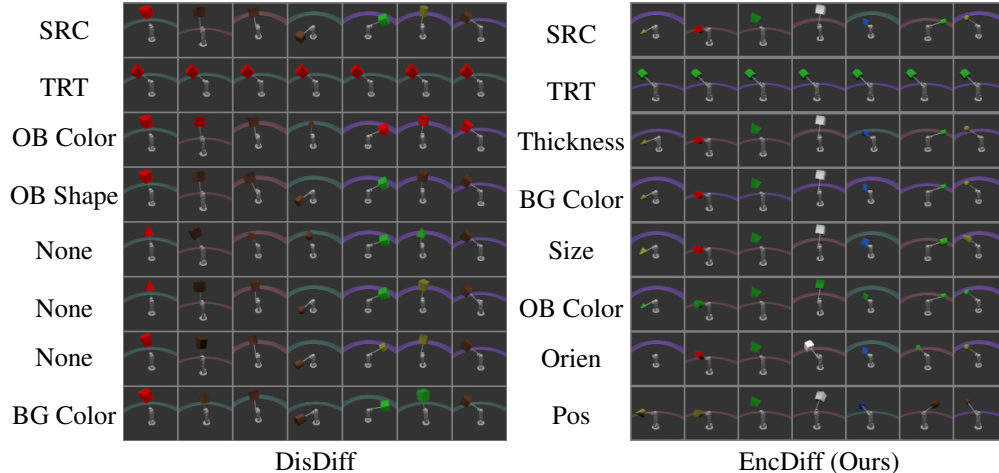
Figure 7: The qualitative results on MPI3D. The source (SRC) images provide the representations of the generated image. The target (TRT) image provides the representation for swapping. Other images are generated by swapping the representation of the corresponding factor. The learned factors on MPI3D are thickness, BG (Background) color, object (OB) color, and object (OB) shape, orientation (Orien), Pos (Background bar position).
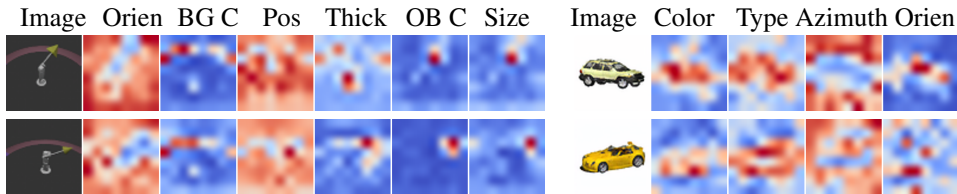

Figure 8: Visualization of the cross-attention maps on MPI3D and Cars3D. The first column shows the original image, while the other columns show the attention masks for different concept tokens.

G Autoencoding Reconstruction Quality

Autoencoding Reconstruction Quality To investigate the autoencoding reconstruction quality of EncDiff, we conduct the same quantitative experiments with PDAE, DisDiff and Diff-AE. We follow them to evaluate the reconstruction quality using averaged SSIM, LPIPS, and MSE. The results are shown in Table 9. It is evident that EncDiff outperforms DisDiff on all metrics. EncDiff achieves the state-of-the-art performance of SSIM and LPIPS with a strong disentanglement capability.

Table 9: Reconstruction quality comparison on the Shape3D dataset.

Method	SSIM↑	LPIPS↓	MSE↓	DCI↑	Factor VAE↑
PDAE	0.9830	0.0033	0.0005	0.3702	0.6514
Diff-AE	0.9898	0.0015	$\mathbf{8.1983e-05}$	0.0653	0.1744
DisDiff	0.9484	0.0006	$9.9293e-05$	0.723	0.902
EncDiff (Ours)	**0.9997**	**0.0003**	$9.6299e-05$	**0.999**	**0.969**

H More Ablation Related with EncDiff

Measuring on Scalar-valued vs. Vector-valued Representations in our EncDiff For EncDiff, each dimension of the scalar-valued representation is mapped to a representation vector, resulting in two representations in EncDiff: a scalar-valued one and a mapped vector-valued one. From Table 10, we can see that these two representations have similar performance.

16

Table 10: Comparison of the two different representations (scalar-valued vs vector-valued) in EncDiff.

Method	FactorVAE score ↑	DCI ↑
EncDiff (Vector)	0.998 ± 0.006	0.955 ± 0.030
EncDiff (Scalar)	$\mathbf{0.999} \pm 0.001$	$\mathbf{0.969} \pm 0.030$

Influence of the Number of Concept Tokens Similar to other disentanglement methods, the number of disentangled latent units influences performance. To study such an effect on EncDiff, we train our model with the following number of tokens: 5, 10, 15, 20 and 30, respectively. As shown in Table 11, when the number of tokens is fewer than the number of ground truth factors, the performance significantly drops. With the use of more tokens, the performance improves. In accordance with the setup proposed by Yang et al. [2022b], EncDiff adopts the default setting of 20 tokens for a fair comparison with other methods Yang et al. [2022b, 2023b], Ren et al. [2021].

Table 11: Influence of the number of concept tokens in EncDiff.

# Tokens	FactorVAE score ↑	DCI ↑
5	0.605 ± 0.084	0.536 ± 0.073
10	0.985 ± 0.032	0.900 ± 0.058
15	0.996 ± 0.015	0.936 ± 0.039
20	$\mathbf{0.999} \pm 0.001$	$\mathbf{0.969} \pm 0.030$
30	0.995 ± 0.014	0.961 ± 0.039

Efficacy of Additional Regularization We are wondering whether additional regularization can further promote the disentanglement. To validate this, we conducted the following experiments to investigate the effectiveness of incorporating two types of constraints: sparsity and orthogonality, respectively.

We explored the orthogonality constraint proposed in Cha and Thiyagalingam [2023], which enforces orthogonality from a group theory perspective. We adapted their method of transforming representations using Euler encoding to enforce orthogonality within EncDiff. We adopted the official implementation on github to modify EncDiff, denoted as EncDiff with Cha and Thiyagalingam [2023]. We integrated the sparsity regularization terms proposed in Fumero et al. [2023] into EncDiff to facilitate disentanglement, denoted as EncDiff with Fumero et al. [2023]. We take the techniques proposed in Yang et al. [2023c], which involve matrix decomposition and matrix exponentiation to construct orthogonal matrices. We replaced the scalar MLP mappings with a series of learnable orthogonal vectors to ensure orthogonality in the representations, denoted as EncDiff with Yang et al. [2023c].The results are shown in Table 12. We observed that the regularization can slightly improve the performance further on our EncDiff. For simplicity, we do not incorporate any regularization on all other results.

Table 12: Ablation study on the additional regularization over EncDiff. We use a CNN encoder by default.

Method	FactorVAE score ↑	DCI ↑
EncDiff w/Cha and Thiyagalingam [2023]	0.999 ± 0.000	0.965 ± 0.040
EncDiff w/Yang et al. [2023c]	0.999 ± 0.002	0.972 ± 0.029
EncDiff w/Fumero et al. [2023]	0.999 ± 0.001	$\mathbf{0.975} \pm 0.031$
EncDiff	$\mathbf{0.999} \pm 0.001$	0.969 ± 0.030

Influence of the Image Encoder Architecture To investigate the influence of encoder design, we use a powerful encoder to replace the CNN encoder used in the EncDiff. We adopt a transformer encoder with a set of learnable tokens as the disentangled representations, as introduced in [Yang et al., 2022b], which are refined through cross-attention. We refer to this scheme *EncDiff w/Trans.* For fair comparison, the model size of the encoders is similar. As shown in Table 13, *EncDiff w/Trans* is comparable to EncDiff. When considering the performance gap between DisDiff Yang et al. [2023b] and our EncDiff, the influence of encoder structures is small and is not the key factor for influencing disentangling capabilities. A similar phenomenon is observed in vector-valued one.

Table 13: Ablation study on image encoder. EncDiff w/Trans denotes the scheme in which we replace CNN encoder with a transformer encoder.

Method	FactorVAE score↑	DCI↑
DisDiff Yang et al. [2023b]	0.902 ± 0.043	0.723 ± 0.013
EncDec w/Trans	0.962 ± 0.034	0.898 ± 0.033
EncDiff	$\mathbf{0.999} \pm 0.001$	0.969 ± 0.030

I More Ablation Study on EncDiff-V

We also perform ablation study related with EncDiff-V to validate the effects of the two inductive bias, the inefficacy of additional regularization. Similar trends as EncDiff are observed.

Ablation on Two Inductive Bias of EncDiff-V In alignment with the main paper, we also conducted an experiment to assess the effectiveness of the two inductive biases in EncDiff-V. We adopt the same decoder used in Section 4.4 to substitute the diffusion in EncDiff-V. We denote this model as EncDec-V w/o Diff. On the other hand, to study the effectiveness of cross-attention, we use the same conditional decoder of EncDiff w/ AdaGN in EncDiff-V, denoted as EncDiff-V w/ AdaGN. The performance of both of these two models drops significantly, as indicated by the results in Table 14.

Table 14: Ablation study on the influence of the two different inductive biases of EncDiff-V. For *EncDec-V w/o Diff*, we replace the diffusion model with a decoder while cross attention is preserved for the interaction. For *EncDiff-V w/ AdaGN*, we replace the cross attention with AdaGN.

Method	FactorVAE score↑	DCI↑
EncDec-V w/o Diff	0.682 ± 0.092	0.246 ± 0.073
EncDiff-V w/ AdaGN	0.956 ± 0.039	0.520 ± 0.083
EncDiff-V	0.999 ± 0.000	0.900 ± 0.045